NeuroImage 174 (2018) 297–307

Contents lists available at ScienceDirect

NeuroImage

journal homepage: www.elsevier.com/locate/neuroimage

The chaotic morphology of the left superior temporal sulcus is genetically constrained

Yann Le Guen [a,*], François Leroy [b], Guillaume Auzias [c], Denis Riviere [a], Antoine Grigis [a], Jean-François Mangin [a], Olivier Coulon [c], Ghislaine Dehaene-Lambertz [b], Vincent Frouin [a,*]

[a] UNATI, Neurospin, Institut Joliot, CEA, Université Paris-Saclay, Gif-sur-Yvette, France
[b] INSERM, UMR992, Neurospin, Institut Joliot, CEA, Université Paris-Saclay, Gif-sur-Yvette, France
[c] Institut de Neurosciences de la Timone, UMR 7289, Aix Marseille Université, CNRS, Marseille, France

ARTICLE INFO

Keywords:
STS asymmetry
Pli de passage
Structural MRI
Imaging genetics
Cortical folding
Heritability

ABSTRACT

The asymmetry of the superior temporal sulcus (STS) has been identified as a species-specific feature of the human brain. The so-called superior temporal asymmetrical pit (STAP) area is observed from the last trimester of gestation onwards and is far less pronounced in the chimpanzee brain. This asymmetry is associated with more frequent sulcal interruptions, named *plis de passage* (PPs), leading to the irregular morphology of the left sulcus. In this paper, we aimed to characterize the variability, asymmetry, and heritability of these interruptions in the STS in comparison with the other main sulci. We developed an automated method to extract PPs across the cortex based on a highly reproducible grid of sulcal pits across individuals, which we applied to a subset of Human Connectome Project (HCP) subjects (N = 820). We report that only a few PPs across the cortex are genetically constrained, namely in the collateral, postcentral and superior temporal sulci and the calcarine fissure. Moreover, some PPs occur more often in one hemisphere than the other, namely in the precentral, postcentral, intraparietal sulci, as well as in both inferior and superior temporal sulci. Most importantly, we found that only the interruptions within the STAP region are both asymmetric and genetically constrained. Because this morphological pattern is located in an area of the left hemisphere related to speech, our results suggest structural constraints on the architecture of the linguistic network.

Introduction

Since hemispheric asymmetry is a fundamental human trait (Toga and Thompson, 2003), a better description of interhemispheric differences in the brain might shed light on human specificity. Recently, it has been shown that the superior temporal sulcus (STS) is deeper in the right hemisphere in most humans irrespective of their age, sex, or handedness, whereas this asymmetry is hardly observed in chimpanzees (Leroy et al., 2015). The location of this asymmetry might make it a macroscopic marker of the brain changes allowing for language and social cognition in our species (DeWitt and Rauschecker, 2012; Frith and Frith, 2007; Pelphrey et al., 2004). Therefore, we aimed to further describe this asymmetry considering not only the depth of this sulcus but also its sulcal interruptions. These interruptions are more frequent in the left sulcus and thus contribute to the interhemispheric difference reported in this sulcus (Leroy et al., 2015; Ochiai et al., 2004).

A sulcal interruption or *pli de passage* (PP) occurs when a transverse gyrus connects the two gyri bordering the sulcus (Gratiolet, 1854). It may potentially interrupt every primary and secondary sulcal structure across the brain. Hardly described in brain atlases, they are reported only when the transverse gyrus is superficial and breaks the sulcus into parts (full interruption) (Ono et al., 1990). However, a PP is often invisible in external views of the cortex when it is buried in the depth of the sulcus. It causes a local elevation of the sulcus floor and hence a decrease in the sulcal depth. PPs are commonly considered as tertiary folds, highly variable, related to the chaotic morphology of sulci, and therefore likely not inherited. However, this assumption could be questioned if one considers the number of sulcal interruptions across brains (Ono et al., 1990), notably in the STS (Ochiai et al., 2004) as well as in the precentral and intraparietal sulci (Zlatkina and Petrides, 2014, 2010). Some authors have also attributed a functional significance to some of these PPs, such as a relation between reading performance and PPs in the occipito-temporal sulcus (Borst et al., 2016). Thus, in this paper, we challenged the view of PPs being highly variable tertiary folds and asked

* Corresponding authors. CEA Saclay, Neurospin Bâtiment 145, 91191 Gif-sur-Yvette Cedex, France.
E-mail addresses: yann.leguen@cea.fr (Y. Le Guen), vincent.frouin@cea.fr (V. Frouin).

https://doi.org/10.1016/j.neuroimage.2018.03.046
Received 14 December 2017; Received in revised form 1 March 2018; Accepted 19 March 2018
Available online 21 March 2018

whether PPs can be robust landmarks, in particular in the STS and possiblu other sulci of the human brain.

Moreover, we also assessed the heritability of PPs in the STS. Gyrification is a heritable trait in primates (Rogers et al., 2010). Kochunov et al. (2010) pinpointed that cortical anatomy is heritable in an extended pedigree of baboons and emphasized that the heritability of sulcal phenotypes might be modulated by the arcuate U-fiber systems. However, Gómez-Robles et al. (2015) underlined that heritability of cerebral cortical anatomy is less important in humans than in chimpanzees. Yet, we have shown that the heritability of sulcal pit depth is mostly symmetric in humans except in the STS (Le Guen et al., 2017b).

PPs are complex shapes difficult to match between subjects, due to the high variability of folding patterns in the cortex. To overcome this difficulty, Régis et al. (2005) developed a model of cortical gyrification based on indivisible units named sulcal pits (or roots), which correspond to the first folding locations. Over the past few years, robust algorithms have been developed to extract these putative primary cortical folding locations (Auzias et al., 2015; Im et al., 2010). These points located at the maximum depth of a sulcal basin show less inter-subject variability than more superficial features and have been proposed as anatomical landmarks (Lohmann et al., 2008). Recent studies on fetal and perinatal MRI data support the assumption that early folding regions are less variable across subjects than other cortical regions (Dubois et al., 2008; Habas et al., 2012). Once sulcal pits are identified within an individual, PPs can then be detected and localized relative to them. Indeed, a sulcal interruption can be seen as a rapid variation in shape of the cortical surface between a pair of neighboring pits.

Thus, we first identified sulcal pits across the brain based upon our earlier study (Le Guen et al., 2017b). Then, we detected PPs between any pair of pits located in the same sulcus, as local variations in the fundus of the sulcus. A function was defined combining both depth and curvature parameters. PPs were considered present if this function reached a given threshold. We applied this method to the Human Connectome Project (HCP) dataset. This enabled us to see whether PPs are reproducible across a large set of individuals and if some are more frequent in one hemisphere or the other. Furthermore, we assessed the genetic control on the presence of PPs with the extended pedigree of 820 Caucasian individuals available in HCP. This pedigree information allowed us to estimate the phenotypic variance explained by the genes' additive effects.

Methods

Subjects

In this work, we used the data from the Human Connectome Project (HCP) S1200 release: details are available in the HCP reference manual. In our analysis, we included 820 subjects (383/437 M/F), labelled as Caucasian with 69 individuals from the Hispanic ethnicity. The pedigree is composed of 191 twin pairs (127 monozygotic (MZ) with 123 siblings, and 64 dizygotic (DZ) with 64 siblings and 1 half sibling), 190 siblings, 1 half sibling and 59 unpaired individuals, aged between 22 and 36 years old ($\mu \pm \sigma = 29.0 \pm 3.6$ years). Unpaired individuals did not contribute to the genetic parameter estimation but allowed for a more accurate estimation of mean and variance effects. Subjects were chosen by the HCP consortium to represent healthy adults beyond the age of major neurodevelopmental changes and before the onset of neurodegenerative changes (Van Essen et al., 2012). They underwent a battery of tests to determine if they met the inclusion/exclusion criteria of the HCP, described in Van Essen et al. (2012). All subjects provided written informed consent on forms approved by the Institutional Review Board of Washington University.

MR image acquisition and image processing

MR images were acquired on a 3 T Connectome scanner, adapted from a Siemens Skyra, housed at Washington University in St Louis using a 32-channel head coil. For T1-weighted images, 256 slices per slab were acquired with the three-dimensional magnetization-prepared rapid gradient echo (3D-MPRAGE) sequence: TR = 2400 ms, TE = 2.14 ms, TI = 1000 ms, flip angle = 8°, FOV = 224*224 mm, and resolution 0.7 mm isotropic. For T2-weighted images, 256 slices per slab were acquired with a 3D-T2SPACE sequence: TR = 3200 ms, TE = 565 ms, variable flip angle, FOV = 224*224 mm, and resolution 0.7 mm isotropic. More details on the acquisition and reconstruction can be found in the HCP S1200 Reference Manual.

Structural images were first processed by the HCP using the HCP structural preprocessing pipeline, whose details can be found in the HCP S1200 Reference Manual. We used the preprocessed T1w and T2w volumes from each individual subject's MR data as input of the HCP Freesurfer pipeline, which is based on Freesurfer 5.3.0 (Fischl, 2012) with a number of enhancements specifically designed to capitalize on HCP data. This step yielded the meshes of the white/grey matter interface for the right and left hemispheres. Then, we performed surface-based interhemispheric registration as proposed in Greve et al. (2013). First, we created the *xhemi* of each subject using the *xhemireg* command of Freesurfer, to transform the right hemisphere into a left one and then computed the registration to the left side of the symmetric Freesurfer template (*fsaverage_sym*) using the *surfreg* command. This transformation will be referred hereafter as the individual spherical interhemispheric registration.

Sulcal pits extraction and group areal definition

We extracted the sulcal pits from the white matter meshes of both hemispheres in the native space for each individual (Auzias et al., 2015; Le Guen et al., 2017a) (Fig. 1a). The procedure first estimated the depth of each vertex on the surface using the depth potential function (DPF) (Boucher et al., 2009). The DPF is a scalar field corresponding to the signed traveled distance, which quantifies how much a curve is bent inward or outward (i.e. average convexity). It represents the overall shape of a fold as the function whose Laplacian is as close as possible to the mean curvature (κ_{mean}) of the surface and is governed by the equation $(\alpha I + \Delta)D_\alpha = 2_{\kappa mean}$, where D_α is the DPF field, α controls the decay rate of the curvature influence as we move further from a given point, and I and Δ represent the identity and the Laplacian matrices respectively. When α tends to infinity, the DPF tends to the mean curvature. When α tends to 0, the DPF tends to the average convexity. Finally, for intermediate values of α, the DPF integrates both types of geometrical information. Thus, the DPF provides a regularized estimation of the depth of the folds and takes into account information from both convexity and curvature (see Auzias et al., 2015; Boucher et al., 2009 for implementation details). For each hemisphere, the DPF is estimated at each vertex of the white matter mesh resulting in a depth map to which we applied a filtered watershed algorithm to obtain the sulcal basins defined from the local DPF maxima. After the extraction of pits at the individual level, we computed the symmetric group-level cluster regions as proposed in Auzias et al. (2015). The smoothed maps from both hemispheres were projected onto the left side of *fsaverage_sym*, and summed across subjects to obtain the group density map (Fig. 1 b). From this density map, group-level clusters of pits denoted hereafter as “areals” were obtained by applying a watershed algorithm as detailed in Auzias et al. (2015) (Fig. 1 c.). Group sulcal pit areals were back-projected onto each subject's hemisphere thereby providing sulcal pit labelling consistent across individuals. The depth profile was then computed in the native space as described in the next section.

Automated sulcal depth profile extraction

We propose a method to automatically extract the sulcal depth profile (SP). The sulcal fundus is the shortest path on the white matter mesh following the extremal values of the DPF between two extremity points. Such a Definition of sulcal fundi has been proposed by Shattuck et al.

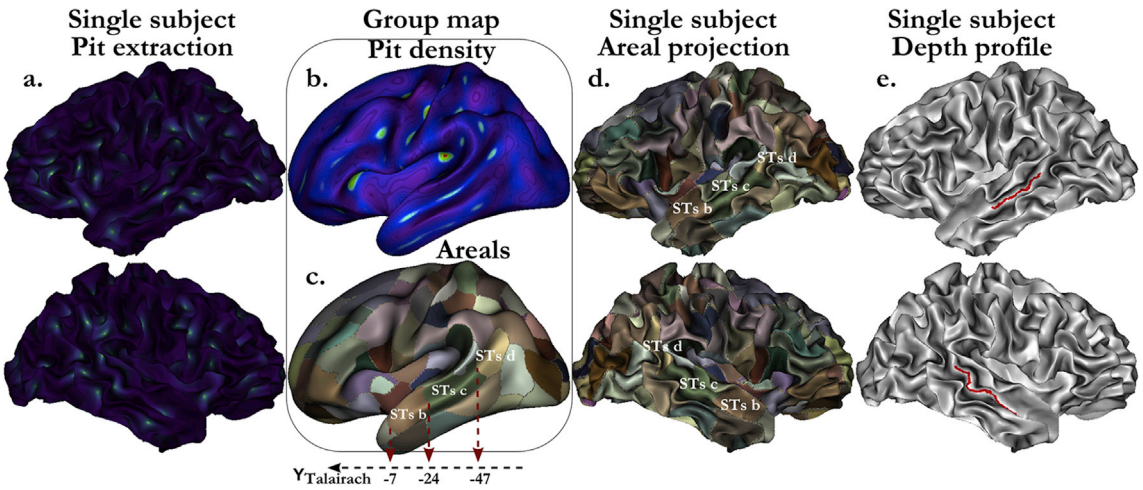

Fig. 1. Summary of the automated pipeline computing the STS depth profile (presented on HCP subject 100307 for "Single subject" steps and on *fsaverage_sym* for the "Group map"). First, the sulcal pits of all subjects are extracted on the cortical surface. Individual smooth pit maps (**a.**) are projected and summed on the symmetric template to obtain the population pit density (**b.**). Areal boundaries (**c.**) are computed with a watershed on the density map. Then, these areals are projected onto each subject's white matter mesh (**d.**). The deepest pits in the areals identified as STs b and STs d, are used as start and end points of the geodesic path following the bottom of the STs. STAP depth profile (**e.**) is then truncated at the border between STs c and STs d.

(2009) and successfully used in Le Troter et al. (2012). They proposed to extract the shortest path between the two extremities on the surface, such as sulcal depth. We used their implementation in our current work. Additionally, we defined the geodesic depth on the white matter mesh as the geodesic distance to the ridges on the crown of gyri in contact with the brain hull (Rettmann et al., 2002). Then, we defined two sulcal depth profiles SP_{DPF} and SP_{GD} representing the DPF and geodesic depth of the vertices along the sulcal fundus geodesic path, respectively.

Our implementation of the sulcal fundus extraction relies on the identification of two extremities, which cannot be performed manually on large datasets such as HCP. In the absence of a clear Definition of the concept of sulcal line extremity, this identification is complex, and inter-individual correspondence is difficult to achieve. In order to provide consistent pairs of extremities able to be defined for each subject, we extended this framework by setting two sulcal pits in specifically chosen areals as the extremities of the sulcal fundus. It is worth emphasizing that we did not extract the SP_{DPF} (and the SP_{GD}) of the whole sulcus but only for a particular segment between these two sulcal pits. As suggested by previous literature (Im et al., 2010; Lohmann et al., 2008; Meng et al., 2014), we assumed anatomical correspondence between the sulcal pits across individuals, which was key to automatizing the SP extraction in a cohort as large as the HCP. In particular, the sulcal pit extraction algorithm proposed in Auzias et al. (2015) is designed to optimize this inter-subject correspondence. Prior to extracting the SP on the native meshes, all areals were projected from the group map onto the subject white matter meshes (left and right) through spherical inter-hemispheric registration (Fig. 1 d.). The group areals represent cluster regions with a high group density of pits. Each group areal name was based on previous literature (Im et al., 2010; Le Guen et al., 2017b; Meng et al., 2014)). Fig. 2 displays the group areal nomenclature for the main sulci. The individual sulcal pits lying in these areals were then automatically identified, and the two deepest pits were used as extremities of the sulcal fundus. In the rare case (<10%) for which one subject had no deep pit in a group areal, the vertex with the maximum DPF was chosen (see SFig. 1 for an example).

We illustrate here the sulcal depth profile extraction process for the STS and, more precisely, in the STAP (Superior Temporal Asymmetrical Pit) area described by Leroy et al. (2015). This sulcus is of particular interest it is consistently deeper in the right hemisphere compared to the left. On the areal group map (Fig. 1), areals corresponding to STS b, c, d were identified as regions 20, 21, 22 in Fig. 2. The STAP includes the areals STS c and partly STS b, according to the Talairach coordinates provided in Leroy et al. (2015), y_{STAP} is between $y \approx -8;-12$ to $-42;-45$. Thus, we extracted the SP_{DPF} and SP_{GD} between the deepest points in STS b and d, since pits b and d are the closest anterior and posterior landmarks, respectively. We truncated it at the border between areals STS c and d, since pit d in the right hemisphere was located posteriorly to the STS in approximately 15% of subjects. Localization errors were mainly due to a slightly shorter STS in this hemisphere compared to the left one. Furthermore, since the coronal coordinate of the border between areals STS c, d is -47 in Talaraich space, it well matched the posterior coordinate of the STAP region. This last remark enabled us to benchmark our method on the data in which the PPs were manually annotated PP from Leroy et al. (2015) by considering a segment as similar as possible to the one they reported.

Pli de passage detection applied in the superior temporal sulcus

Visual inspection of the data revealed that the left STS is often segmented in smaller sections by PPs. To extract the PPs, one method would consist in computing a watershed on the reverse depth map compared to the one used to identify the sulcal pits. However, the PPs might be difficult to disentangle from the noise of adjacent gyri. The second option would be to extract PPs from the sulcal depth profiles

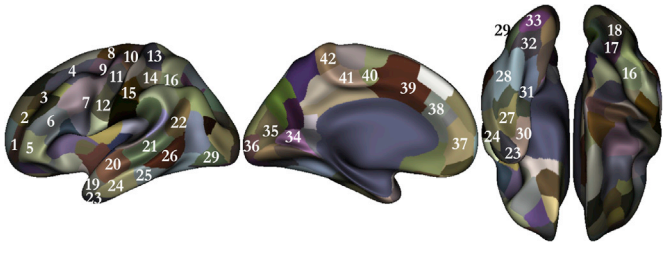

Fig. 2. Areal nomenclature: 1 sup frontal a, 2 sup frontal b, 3 sup frontal c, 4 sup frontal d, 5 inf frontal a, 6 inf frontal b, 7 inf frontal c, 8 precentral a, 9 precentral b, 10 central a, 11 central b, 12 central c, 13 postcentral a, 14 postcentral b, 15 postcentral c, 16 intraparietal a, 17 intraparietal b, 18 intraparietal c, 19 sup temporal a, 20 sup temporal b, 21 sup temporal c, 22 sup temporal d, 23 inf temporal a, 24 inf temporal b, 25 inf temporal c, 26 inf temporal d, 27 occipito-temporal a, 28 occipito-temporal b, 29 occipito-temporal c, 30 collateral a, 31 collateral b, 32 collateral c, 33 collateral d, 34 calcarine a, 35 calcarine b, 36 calcarine c, 37 cingulate a, 38 cingulate b, 39 cingulate c, 40 cingulate d, 41 cingulate e, 42 cingulate f.

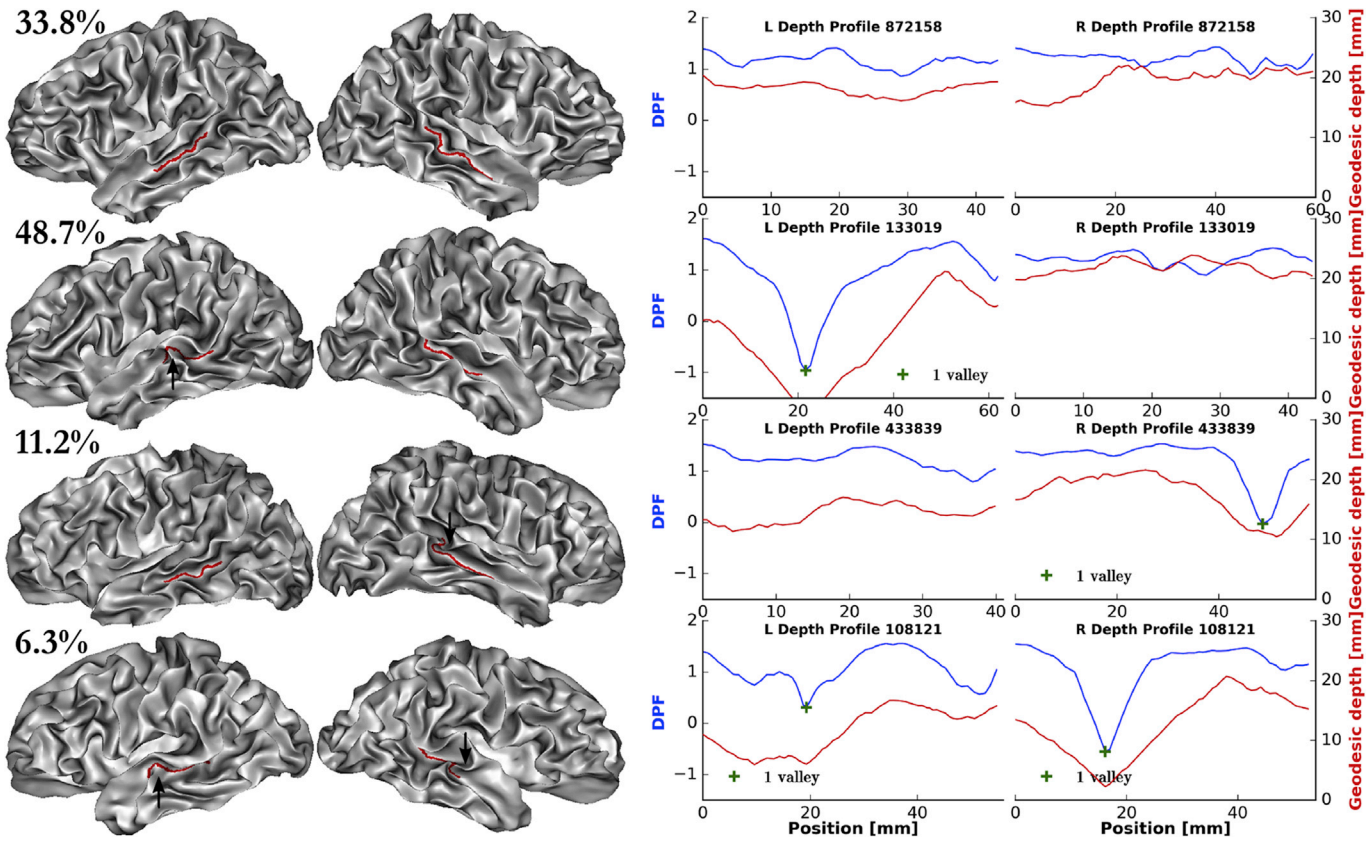

Fig. 3. Typical STAP patterns with either symmetric STAP with no PPs on either side (1st line: 33.8% of HCP Caucasians subjects) or one PP on each side (4th line: 6.3%), or asymmetric STAP with only one PP on the left (2nd line: 48.7%) or on the right (3rd line: 11.2%). The associated depth profiles in the STAP are shown on the right of the figure. Black arrows indicate the pli de passage position on the mesh. The subjects' white matter meshes have been slightly inflated and smoothed to allow a clearer view of the extracted geodesic path. SFig. 11 shows the average depth profile in the STAP for each configuration.

computed between the sulcal pits (used as the extremities of the sulcal fundus), as these are more stable across individuals. It should be noted that for the SP_{DPF} and SP_{GD} functions, peaks correspond to the maximum depth while low valleys represent PPs. Valleys were detected as local minima along sulcal depth profiles (Fig. 3) with a constraint on both the minimum gap between two valleys and minimum DPF height of the valley floor. In order to assess the best threshold of the minimum SP_{DPF} in the STAP, we measured the SP_{DPF} minima in all valleys computed across all subjects to establish its empirical distribution. This distribution was fit with a mixture of two Gaussians with low and high SP_{DPF} values corresponding to PPs and noise in the depth profiles, respectively (SFig. 2). Noise was removed using a standard 3σ threshold from the high Gaussian distribution (true PPs have $SP_{DPF} \leq 0.42$).

To improve detection, we also used SP_{GD} to assess how superficial a PP is. To set a threshold on the SP_{GD} and evaluate the pertinence of the SP_{DPF} one, we assessed our recognition method on manually labelled data outside the HCP from (Leroy et al., 2015). With SP_{DPF} and SP_{GD} thresholds set at 0.42 and 13 mm, respectively, we obtained a concordance of 80% between the reported presence/absence of PP in the STAP of 98 individuals (196 hemispheres).

To assess the robustness of these ad hoc parameters, we estimated the accuracy, sensitivity and specificity of our method using a grid of threshold parameters ($SP_{DPF} \times SP_{GD}$, with SP_{DPF} varying from −0.5 to 1.0, and SP_{GD} from 5.0 mm to 20.0 mm) on the previous 196 hemisphere dataset. The maximum accuracy (82%) was obtained with $SP_{DPF} = 0.08$ and $SP_{GD} = 11.8$ mm as thresholds. The accuracy slightly increased as compared to the previous set of parameters, and we noticed that the sensitivity decreased from 50% to 40.5%, while the specificity increased from 64.1% to 75% (SFig. 3). Overall, setting the SP_{DPF} threshold in the range 0–0.5 gave similar accuracy and a reasonable trade-off between sensitivity and specificity.

Furthermore, we looked into the causes of discordant cases and found that they were mostly due to two reasons. First, our delimitation of the STAP was sometimes longer or shorter than the reference. This is particularly difficult to reproduce in an automated process due to the manual identification of the planum landmark used in (Leroy et al., 2015). Secondly, some cases seemed to have been manually misidentified due to a slightly different procedure used at the time of identification with Brainvisa (Mangin et al., 2015; Perrot et al., 2011). After visual inspection of the PP detection in the HCP dataset, the first set of parameters ($SP_{DPF} = 0.42$ and $SP_{GD} = 13$) mm was chosen and proved to extract the PPs robustly.

To summarize, PPs were extracted in three steps: (i) extraction of the sulcal fundus between two extremal sulcal pits in a chosen sulcus; (ii) extraction of the sulcal depth profile along the sulcal fundus; (iii) detection of the PP when the sulcal depth profile reached a minimum DPF and geodesic depth value as previously defined.

Definition of sulcal depth profile extremities to extract the plis de passage

Plis de passage can be extracted between any pair of adjacent sulcal pits (i.e. located in adjacent group sulcal basins) using the corresponding two sulcal pits as extremities of the sulcal depth profile. Indeed, in the sulcal pit theory, two adjacent sulcal pits in a sulcus are separated by a more or less visible bump (PP) between the two. Our approach was dedicated to identifying the bumps that were prominent enough to create a significant interruption of the sulcus. Thus, the extraction of PPs previously described for the STAP was also able to be applied to several major sulci provided that pairs of sulcal pits were able to be used as sulcal fundus extremities. We analyzed the superior and inferior frontal, the

precentral, the central, the postcentral, the intraparietal, the superior and inferior temporal, the occipito-temporal, the collateral, the calcarine and the cingulate sulci (Fig. 2). We restricted our analysis to these sulci as they are composed of at least two adjacent areals, even though some of their segmentations, such as for the occipito-temporal sulcus, could have been manually improved.

Quantifying the hemispheric asymmetry of plis de passage

We defined the asymmetry of plis de passage as: Asym = L – R, where L and R are the percentage of plis de passage in the left and right hemispheres, respectively. We studied the asymmetry of PPs using the Fisher exact test, with Table 1 as contingency table.

Table 1
Contingency table use for the Fisher exact test to quantify pli de passage asymmetries. L0 R1: number of subjects with a PP solely on the right; L1 R0: number of subjects with a PP only on the left; L0 R0: number of subjects without PPs; L1 R1: number of subjects with a PP in both hemispheres. This test statistically assesses whether there is an asymmetric preference towards one hemisphere.

	Asymmetric configurations	Symmetric configurations
Nb of subjects with no PP on the left	L0 R1	L0 R0
Nb of subjects with PPs on the left	L1 R0	L1 R1

Comparison with an existing method: vertex-wise asymmetry using a symmetric template

We compared our result with a vertex-wise approach to detect the asymmetries of Freesurfer cortical thickness and sulcal depth (Chiarello et al., 2016; Fischl, 2012; Maingault et al., 2016; Toga and Thompson, 2003). We projected all individuals' hemispheres onto the left hemisphere of the symmetrical template and performed a *t*-test between the value at each vertex, considering the distribution to be independent across hemispheres. As opposed to sulcal depth, cortical thickness was not directly linked to our PP analysis; however this enabled us to verify if the HCP cohort and our vertex-wise analysis method allowed us to identify the asymmetries already reported in the literature.

Heritability computation

The presence or absence of PPs in various sulci was considered as a phenotype in a heritability study. The variance components method, as implemented in the Sequential Oligogenic Linkage Analysis Routines (SOLAR, http://solar-eclipse-genetics.org/) (Almasy and Blangero, 1998), was used for the heritability estimations of the presence PP in the considered segment. The between subjects covariance matrix Ω for a pedigree of individuals is given by: $\Omega = 2\cdot\Phi\cdot\sigma_g^2 + I\cdot\sigma_e^2$, where σ_g^2 is the genetic variance due to the additive genetic factors, Φ is the kinship matrix representing the pair-wise kinship coefficients among all individuals, σ_e^2 is the variance due to individual-specific environmental effects, and I is the identity matrix, assuming all environmental effects

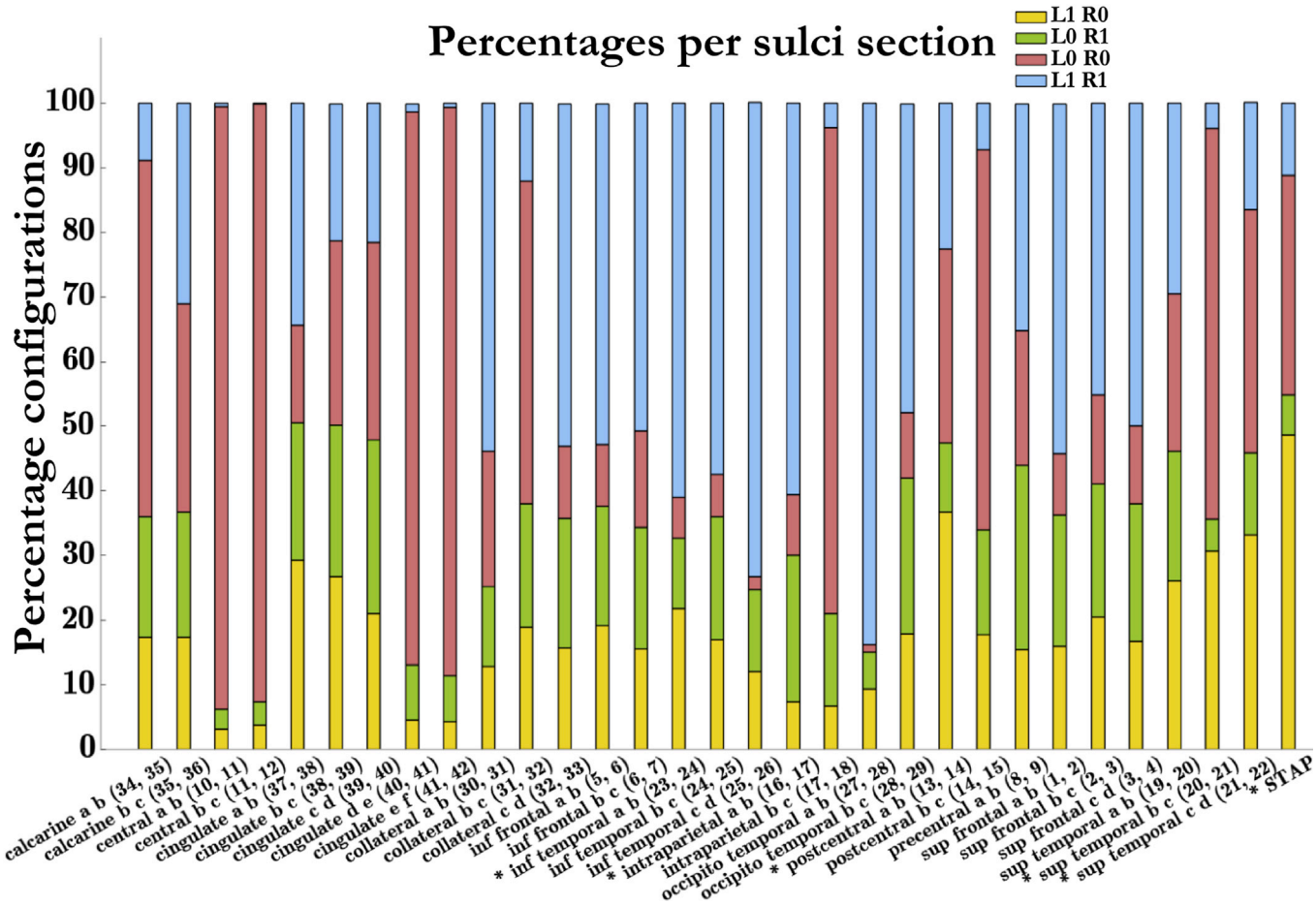

Fig. 4. Percentage of each configuration of pli de passage per sulci section. L1 R1 (blue): proportion of subjects with a pli de passage in both hemispheres for this section; **L0 R0 (yellow)**: without plis de passage; **L1 R0 (green)**: a pli de passage solely in the left hemisphere; **L0 R1 (red)**: solely in the right hemisphere. STable 1 provides the exact percentages used to create this chart. Significantly asymmetric segment names are emphasized with * (see also STable 2.).

are uncorrelated among family members. Narrow sense heritability is defined as the fraction of the phenotype variance σ_p^2 attributable to additive genetic factors: $h^2 = \sigma_g^2/\sigma_p^2$. Significance of the heritability is tested by comparing the likelihood of the model in which σ_g^2 is constrained to zero with that of a model in which σ_g^2 is estimated. Before testing for the significance of heritability, phenotype values for each individual within the HCP cohort were adjusted for the following covariates: sex, age, age^2, age·sex interaction, age^2·sex interaction, ethnicity (Hispanic or not), total intracranial volume, and handedness (measured by Edimburg test (Schachter et al., 1987)).

Relationship between intracranial volume and plis de passage in the STAP

Larger brains are known to be more folded (Germanaud et al., 2012; Toro et al., 2008). Thus, we studied to what extent the presence of a PP in the STAP is related to brain volume. We assessed the potential link between the recognition of a PP and brain volume, approximated by the Freesurfer estimated total intracranial volume (eTIV), using the Mann Whitney statistical test. In addition, we added the eTIV as a covariate in our heritability analysis to assess its significance.

Results

Asymmetry of plis de passage in the STAP

We extracted the sulcal pits, the depth profile, and *plis de passage* in the STS area in 820 subjects of the HCP cohort using the sulcal pits as anatomical landmarks. Fig. 3 displays four typical depth profiles observed in the STAP. Our results show that most subjects (48.7%) had at least one PP solely in the left STS, while few (11.2%) had this configuration only in the right STS. When a PP was detected only in the right hemisphere, it mostly lied at the junction between the STS main horizontal branch and its caudal branch. Remaining subjects had a roughly symmetric STS organization with either no PPs on either side (33.8%) or one PP on each side (6.3%).

Extrapolation of pli de passage detection to quantify asymmetries

We applied our previously described PP detection method between any two adjacent pits in other sulci (see section Definition of sulcal depth profile extremities to extract the plis de passage). Compared to the 42.3% asymmetry of the STAP, all segments had lower asymmetries of PP, and most of them were almost symmetric in terms of PP frequency (Fig. 4, Table 2). Six segments were nevertheless found significantly asymmetric according to the Fisher exact test. They included the STS segments (b, c, asym PP = +25.9%) and (c, d, +20.5%), whose combination partly corresponds to the asymmetry of the STAP. Other asymmetric sulci segments consisted of the inferior temporal (a, b, +11%), intraparietal (a, b, −15.4%), postcentral (a, b +26%), and precentral (a, b, −13%) sulci. Our results also emphasize the generally continuous aspect of the central sulcus with few prominent PPs identified (about 3–4% on each hemisphere for the central sulcus in two segments). It should be noted the well-known PP roughly corresponding to the hand area in the central sulcus is most often deeply buried in the sulcus and was thus not detected by our analysis.

To allow the reader to have a clearer view of the local morphology of the three most asymmetric segments apart from the STS, we present typical subjects for each configuration. Fig. 5 introduces the typical configurations in the postcentral a b (13, 14), intraparietal a b (16, 17) and precentral a b (8, 9) segments. Detailed depth profiles for each of these configurations are respectively shown on SFigs. 4–7. This pipeline can also be applied to identify rare individuals who have a divided central sulcus (Fig. 5), estimated to be about 1% (Ono et al., 1990; Schweizer et al., 2014). Our pipeline identified about 3% of all hemispheres due to noise but can aid neuroanatomists who want to identify these particular subjects to considerably restrain their search.

Table 2
Pli de passage configuration percentages in all considered segments between any two adjacent pits in the main sulci. Numbers within parentheses correspond to nomenclature Fig. 2. An asym >0 corresponds to L > R.

	Asym PP	p-val	L PP	R PP
calcarine a b (34, 35)	−1.3%	0.76	26.2%	27.6%
calcarine b c (35, 36)	−2.2%	0.42	48.3%	50.5%
central a b (10, 11)	0.1%	1.0	3.7%	3.5%
central b c (11, 12)	0.2%	1.0	3.9%	3.7%
cingulate a b (37, 38)	7.9%	0.02	63.7%	55.7%
cingulate b c (38, 39)	3.4%	0.38	48.0%	44.6%
cingulate c d (39, 40)	−5.7%	0.11	42.7%	48.4%
cingulate d e (40, 41)	−3.9%	0.23	6.0%	9.9%
cingulate e f (41, 42)	−2.8%	0.51	4.9%	7.7%
collateral a b (30, 31)	0.4%	0.88	66.7%	66.3%
collateral b c (31, 32)	−0.2%	1.0	31.0%	31.2%
collateral c d (32, 33)	−4.3%	0.08	68.8%	73.0%
inf frontal a b (5, 6)	0.6%	0.84	71.8%	71.2%
inf frontal b c (6, 7)	−3.2%	0.19	66.3%	69.5%
inf temporal a b (23, 24)	11.0%*	$9.0{\cdot}10^{-7}$	82.8%	71.8%
inf temporal b c (24, 25)	−2.1%	0.42	74.4%	76.5%
inf temporal c d (25, 26)	−0.5%	0.82	85.5%	86.0%
intraparietal a b (16, 17)	−15.4%*	$1.6{\cdot}10^{-13}$	67.9%	83.3%
intraparietal b c (17, 18)	−7.7%	0.01	10.5%	18.2%
occipito temporal a b (27, 28)	3.7%	0.01	93.2%	89.5%
occipito temporal b c (28, 29)	−6.1%	0.03	65.7%	71.8%
postcentral a b (13, 14)	26.0%*	$3.8{\cdot}10^{-15}$	59.3%	33.3%
postcentral b c (14, 15)	1.5%	0.74	24.9%	23.4%
precentral a b (8, 9)	−13.0%*	$8.3{\cdot}10^{-6}$	50.7%	63.8%
sup frontal a b (1, 2)	−4.3%	0.08	70.1%	74.4%
sup frontal b c (2, 3)	0.0%	1.0	65.6%	65.6%
sup frontal c d (3, 4)	−4.6%	0.07	66.6%	71.2%
sup temporal a b (19, 20)	6.1%	0.05	55.6%	49.5%
sup temporal b c (20, 21)	25.9%*	$1.2{\cdot}10^{-9}$	34.8%	8.9%
sup temporal c d (21, 22)	20.5%*	$7.2{\cdot}10^{-9}$	49.8%	29.3%
STAP	42.4%*	$3.3{\cdot}10^{-24}$	59.9%	17.6%

Asym PP: hemispheric asymmetry of plis de passage in this section; **L PP:** proportion of subjects with a pli de passage in the left hemisphere in the considered section; **R PP:** respectively in the right hemisphere.
*significant asymmetry for Fisher exact test with $p < 0.001 \approx 0.05/31$ (Bonferroni correction).

Comparison with asymmetries found via vertex wise analysis of sulcal depth and cortical thickness

Traditional methods to assess structural asymmetry use a vertex-wise analysis projecting individual vertex values onto a group template corresponding to an average brain. These approaches are relevant to quantifying differences across hemispheres in terms of sulcal depth, cortical thickness, or cortical surface area and have been widely used in the past (Koelkebeck et al., 2014; Li et al., 2015; Maingault et al., 2016). They do not inform on the local shape along the sulci, such as the detection of a PP. However, there is a close relationship between sulcal depth and the presence of a PP, meaning that hemispheric asymmetry in the frequency of PP should translate to an asymmetry in sulcal depth. The asymmetry in sulcal depth Fig. 6 shows that the right postcentral (a,b) is on average significantly deeper than the left (in red), while the left intraparietal (a,b) is deeper than the right. These results confirm the asymmetry we found in term of PPs in the postcentral (a,b) (+26%) and intraparietal (a,b) (−15.4%) segments. The asymmetries in the precentral (a,b) and inferior temporal (a,b) segments are not reflected by these data. In terms of cortical thickness (CT), the 2nd line of Fig. 6 emphasizes traditionally reported areas, mainly including the rightward asymmetry CT in the STS and its surrounding gyri.

Relationship between the presence of PPs and intracranial brain volume

Larger brains are known to be more folded (Germanaud et al., 2012; Toro et al., 2008) and brain volume is known to be highly heritable (Bartley et al., 1997; Peper et al., 2007). It therefore appears important to assess to what extent the presence of a PP in the left STAP is related to

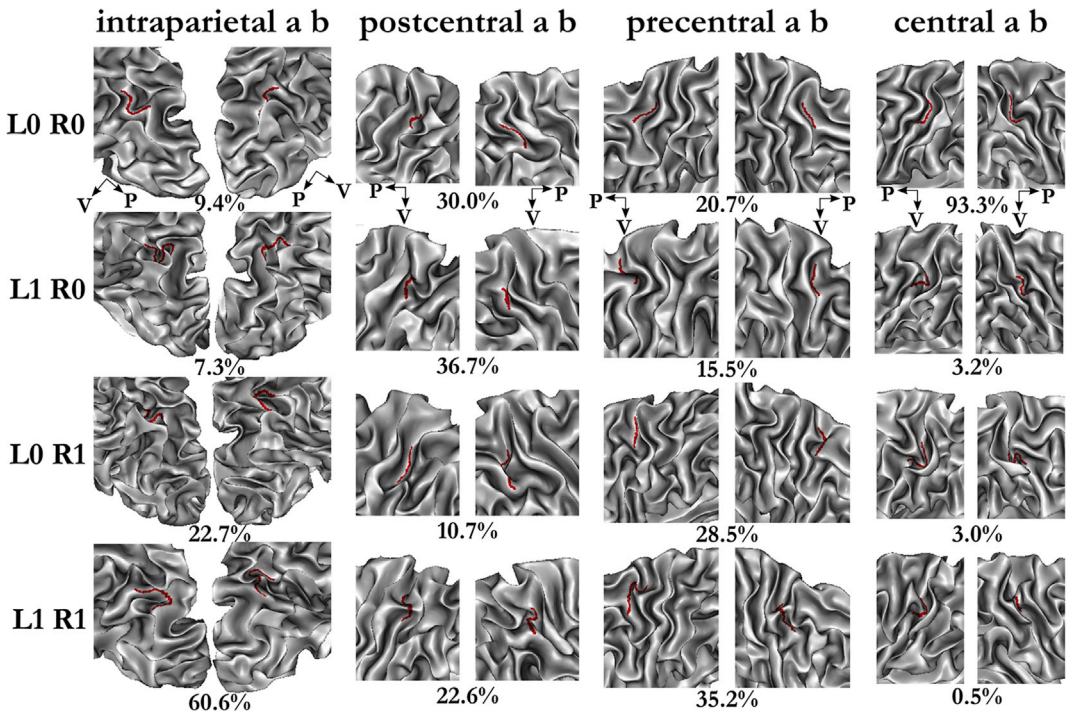

Fig. 5. Typical patterns for each configuration in the intraparietal a b (16, 17), postcentral a b (13, 14), precentral a b (8, 9), central a b (10, 11). L0 R0: no PPs in either hemisphere, L1 R0: A PP in the left hemisphere, L0 R1: A PP in the right hemisphere, L1 R1: PPs in both hemispheres. P and V axes indicate the posterior and ventral directions, respectively.

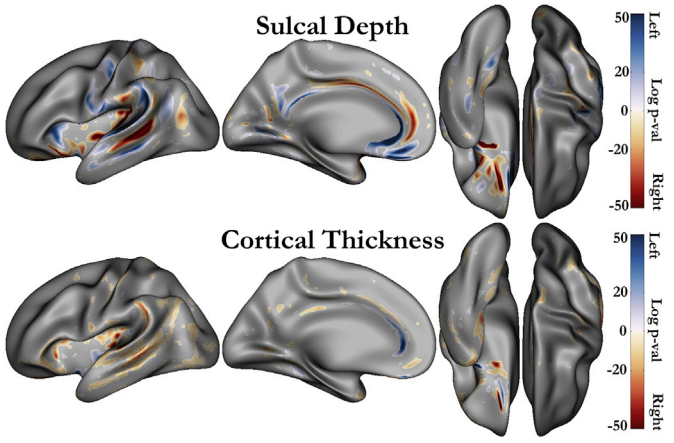

Fig. 6. Log p-values of the *t*-test assessing the asymmetry vertex-wise of sulcal depth and cortical thickness distributions. Only significant asymmetries after Bonferroni correction ($p < 0.05/163842 \approx 3{\cdot}10^{-7}$, where 163842 is the number of vertices on the mesh) are displayed. Blue regions correspond to leftward asymmetries, and red regions, to rightward asymmetries.

brain volume. The logistic regression between the intracranial volume and PPs displayed a small trend with the probability of PPs slightly increasing with brain volume. In our sample, the mean intracranial volume was 1604 cm^3 ($\sigma = \pm$ 176 cm^3), and this probability increased by 0.046 per standard deviation. We applied the Mann-Whitney test to compare the mean intracranial volume distributions for individuals with and without PPs in the STAP. We obtained a significant, yet relatively low p-value of 0.001 for the dataset size. Overall, larger brains were slightly more likely to have a PP in the STAP, but we are unable to set any thresholds on brain volume to consistently confirm the presence or absence of PPs in the STAP. In addition, we performed these tests separately considering the hemispheric white and grey matter volumes and obtained similar results. Thus, we concluded that PPs in the STAP were not directly related to brain or hemispheric volume.

Heritability of the plis de passage

We found a significant heritability estimate for the presence of PPs in the left hemisphere STAP ($h^2 = 0.53$, $p = 10^{-7}$), whereas that for the right hemisphere did not reach significance ($h^2 = 0.26$, $p = 0.03$) (Table 3.). Taking into account all sulci segments in both hemispheres the Bonferroni threshold was set to $p < 0.05/(31*2) \approx 8.1{\cdot}10^{-4}$. To compare the proportion of genetic additive effects found in the STAP, we additionally estimated the heritability for other sulci segments (STables 3, 4). Those significant after correction were the left collateral a b ($h^2 = 0.33$, $p = 10^{-4}$), the left superior temporal b c ($h^2 = 0.33$, $p = 10^{-4}$), the right calcarine b c ($h^2 = 0.48$, $p = 10^{-6}$), the right collateral c d ($h^2 = 0.38$, $p = 10^{-4}$) and the right postcentral b c ($h^2 = 0.37$, $p = 10^{-4}$). It should be noted that most of these estimates had larger standard errors (see STables 3, 4) due to ill balanced classes (i.e., either too large a proportion of subjects with or without PPs). One interesting point to emphasize is that

Table 3
Heritability estimates for the presence of a *pli de passage* in the STAP in both hemispheres. The p-values associated to covariates related to Age, Sex, ethnic group (Hispanic), eTIV and Handedness are also displayed.

Trait	$h^2 \pm SE(p)$	Age	Age^2	Sex	Age*Sex	Age^2*Sex	Hisp.	eTIV	Hand
		p-val							
PP in the Left STAP	0.53 ± 0.09 ($1.0{\cdot}10^{-7}$)	0.49	0.19	0.06	0.73	0.76	0.4	0.21	0.3
PP in the Right STAP	0.27 ± 0.15 (0.03)	1.0	0.69	0.85	0.92	0.93	0.8	0.36	0.33

the STS b-c was the only segment with significant asymmetry and heritability in the left hemisphere. Another interesting finding is that the handedness covariate was only significant for the right postcentral a b segment ($p = 5.5{\cdot}10^{-3}$), which indeed corresponds to the hand knob location.

Exploratory analysis for functional significance of the STAP asymmetry

We found several areals of the HCP multi-modal parcellation (Glasser et al., 2016) whose brain activations in HCP Language task had noticeable correlations ($p < 0.005$, uncorrected) with the depth asymmetry index in the STAP (see SMethod 1, SFigs. 9 and 10). These areals corresponded to the Area STS dorsal (STSd) posterior, ParaBelt Complex, Area Temporo-Parieto-Occipital Junction 2 and VentroMedial Visual Area 3 (STables 5-6). Among these only the STSd posterior had a p-value ($p \approx 8{\cdot}10^{-5}$) that survived a strict Bonferroni correction from the 180 areals per hemisphere ($p < 0.05/(2*180) \approx 5.5{\cdot}10^{-4}$). This finding is interesting as a similar study on the STS asymmetry had not found any structural-functional correlations with a smaller sample (18 subjects) (Specht and Wigglesworth, 2018).

Regarding the correlation of the depth asymmetry index with the HCP cognitive scores, only that for Verbal Episodic Memory Reaction Time (for correct responses) was significant ($\rho = 0.078$, $p = 0.03$, uncorrected, STable 7). This result might emphasize the link between hemispheric specification and cognitive efficiency in support of Ringo's theory (Ringo et al., 1994).

Discussion

Thanks to a new method, we were able to study auxiliary cortical folds, called plis de passage (PPs), in a robust manner across a large cohort. We first observed that few of them are genetically constrained and, second, that some of them occur more often in one hemisphere than in the other. Finally, we found that only one PP is both asymmetric and genetically constrained across the cortex. This PP is located in the intermediate segment of the STS, the so-called STAP region.

The observation that a PP often divides the left STS within the STAP region is in agreement with the reported rightward asymmetry of the STS depth profile (Bodin et al., 2017; Glasel et al., 2011; Leroy et al., 2015), and contributes to this asymmetry to a large extent (Leroy et al., 2015; Ochiai et al., 2004). Furthermore, this interruption is part of a heritable morphological pattern along the left STS concerning the neighboring sulcal pits in areals b and c, which are also heritable (Le Guen et al., 2017b). Thus, the interruption in between the pits STS b-*c*-d forms a saddle-like shape under genetic constraints in the left STS. This rather complex conformation, which is the only one both asymmetrical and heritable across the cortex, suggests an evolutionary pressure in this region. Whereas the right STS lacks a PP between pits b and c.

Several asymmetries are present in the superior temporal region that may participate in this particular shape. First, the prominence of PPs in the left hemisphere may reflect an asymmetry in white-mater connectivity, which shapes the cortical surface (Hilgetag and Barbas, 2006). Numerous long-range tracts, namely the arcuate fasciculus, the middle longitudinal fasciculus, the inferior occipito-frontal fasciculus, and transcallosal fibers (Turken and Dronkers, 2011), cross in this region and intermingle with a dense local connectivity (Mesgarani et al., 2014). Among them, the left arcuate fasciculus is larger than the right already early on in life (Dubois et al., 2015). In addition, PPs might also materialize the U-shape fibers which mediate short intralobar connectivity as it might be the case in the central region (Catani et al., 2012; Zhang et al., 2014). Catani et al. (2012) have shown that the fiber connections between the hand-knob motor region and the postcentral gyrus are left lateralized. The left asymmetry we found in the postcentral a b segment is in agreement with this left lateralization. Second, the preferential formation of PPs in the left STAP might be caused by left-right differences in maturational rate, which is thought to play a decisive role in creating structural and functional lateralization in the human brain (de Kovel et al., 2017). Indeed, the right STS appears earlier during gyral development than the left STS (Chi et al., 1977) and matures faster (Leroy et al., 2011). Finally, we cannot exclude a difference in neuronal proliferation in left and right STS progenitors leading to a differential growth between grey and white matter (de Juan Romero et al., 2015; Tallinen et al., 2016) and thus to supplementary tertiary folds when synaptic trees develop. The observation in adult post-mortem brains that the superficial layers of the left superior temporal cortex contain a greater number of large pyramidal cells than the right (Hutsler, 2003) might be part of this specific gyral conformation.

What is the relation between this anatomical pattern and human cognitive functions? The STS is a key structure in voice and face recognition, biological motion, theory of mind, audio-visual integration and language (Deen et al., 2015; Hein and Knight, 2008) with robust functional asymmetries. Although a clear functional subdivision along the sulcus is still debated, the location of the STAP at the basis of Heschl's gyrus points towards a role in vocal stimuli processing (Deen et al., 2015), voice recognition in the right hemisphere (Belin et al., 2000; Moerel et al., 2012) and speech processing in the left hemisphere (DeWitt and Rauschecker, 2012). Since heritability was found only in the left hemisphere, genetic constraints would be stronger on the structural organization of speech network, either within the auditory domain or within the auditory-visual connections. Indeed, the middle STS is the first linguistic step in converting acoustic features into phonemes (DeWitt and Rauschecker, 2012; Liebenthal et al., 2010; Mesgarani et al., 2014) and entering the hierarchy of areas sensitive to increasing levels of linguistic structures (Dehaene-Lambertz et al., 2006; Pallier et al., 2011). It is also the site of auditory and visual cross-modal integration (lip-reading (Calvert et al., 1997; Nath and Beauchamp, 2012; Paulesu et al., 2003), communicative gestures (Redcay et al., 2016), sign language (Moreno et al., 2018; Neville et al., 1998), as well as graphene-phoneme conversion (Dehaene et al., 2010)). We tentatively explored the structure-function relationship by taking into account the functional tasks tested in the HCP. We observed a significant and large correlation between the activations in the story and math tasks and the asymmetry index in the middle-posterior STS. Again, this asymmetry driven by the left hemisphere indicates that the linguistic component of these tasks might be the crucial factor related to the STAP (SFigs. 9 and 10).

The larger heritability in the left STS implicates genes involved in language circuits as the first candidates, such as FOXP2, linked to language lateralization (Ocklenburg et al., 2013), and KIAA0319, whose haplotypes have been shown to correlated with asymmetry of activation in the STS (Pinel et al., 2012). Genome wide association studies of these phenotypes (GWAS) have yielded few significant results because they require enough statistical power to detect variants with small effect sizes. Another interesting approach to identify genes involved in language lateralization would be to focus on genes expressed asymmetrically in both hemispheres (Karlebach and Francks, 2015; Sun and Walsh, 2006). In particular, those differentially expressed in perisylvian speech and language regions during fetal development should be considered (Johnson et al., 2009). Epigenetic modifications in gene expression, such as DNA methylation, histone modification, as well as modulation of expression, such as microRNA post-transcriptional regulation, also need to be examined (Güntürkün and Ocklenburg, 2017). Our pipeline, which robustly and automatically extracts brain asymmetrical features, such as *plis de passage*, should help in investigating the implicated biological pathways in large cohorts.

Other hemispheric asymmetries

The other asymmetries that our results revealed are in agreement with neuro-anatomical descriptions in the STS (Ochiai et al., 2004), the postcentral sulcus (Zlatkina and Petrides, 2010) and the intraparietal sulcus (Zlatkina and Petrides, 2014). In 40 subjects, Zlatkina and Petrides closely delineated the postcentral sulcus segments corresponding to the

those of the sulcal roots theory (Régis et al., 2005). We found that the left postcentral sulcus contained more interrupting gyri, notably in its dorsal part, which is concordant with their report. Looking at their drawing of the postcentral and adjacent sulci, we speculate that the asymmetric interruption we quantified might be due to the ascending (marginal) branch of the cingulate sulcus that merges in the postcentral sulcus superior part. In their second study, these authors emphasized that the intraparietal sulcus is divided by a submerged gyrus into two branches, the anterior ramus and the posterior ramus (Zlatkina and Petrides, 2014). They confirmed the trend we found by underlining that the gyral passage occurred more often in the right hemisphere. Third, Shen et al. (2018) reported a significant rightward sulcal depth asymmetry in the anterior cingulate sulcus in normal elderly individuals. This asymmetry is confirmed both by our vertex-wise analysis (Fig. 6) and by a 7.9% increase in the amount of left PPs between anterior cingulate pits a and b. Fourth, we did not find any PP asymmetry in the collateral sulcus, as reported in a manual neuroanatomical study (Huntgeburth and Petrides, 2012). Finally, we underlined new findings which need to be further investigated. First, there are more sulcal interruptions in the left infero-temporal region and the right precentral region than in the contralateral hemisphere; asymmetry size is larger than 10%, which is a commonly used threshold to assess brain asymmetry (Galaburda et al., 1987). Second, we reported significant heritability of sulcal interruptions in the left collateral sulcus, the right calcarine fissure, the right collateral sulcus, as well as in the right postcentral sulcus. Our asymmetry results were confirmed by our vertex-wise analysis of the sulcal depth asymmetry. This second approach emphasized rightward asymmetries of sulcal depth in the dorsal postcentral, as well as leftward asymmetry in the intraparietal and on precentral gyrus.

It is difficult to compare our study with previous automated studies of cortical asymmetry as they mainly focused on cortical thickness and cortical surface area. Surface based approaches are twofold either using a cortex parcellation (Chiarello et al., 2016; Kang et al., 2015), in particular the automated Freesurfer ones (Destrieux et al., 2010), or considering interhemispheric registration (Maingault et al., 2016) as we did for our vertex-wise analysis. Overall, we agree with the rightward asymmetry of cortical thickness in the superior temporal lobe (Maingault et al., 2016). Sulcal depth asymmetry has rarely been studied cortex-wise, but previous literature has emphasized a rightward asymmetry in the superior temporal sulcus (Maingault et al., 2016; Van Essen, 2005) and a leftward asymmetry for right handers in the precentral area corresponding to the Rolando genu (Maingault et al., 2016) similar to our result (Fig. 6). We assume they did not observe the other asymmetries in sulcal depth due to either smaller samples or differences in the methodology such as the registration technique in (Van Essen, 2005). Moreover, Maingault and colleagues performed a questionable 10 mm FWHM (full width half maximum) Gaussian filter on each subject asymmetry map. This filtering likely blurred out some population asymmetries, keeping only the largest.

Our study is the first to propose an automated extraction of prominent transverse gyri, the so-called *plis de passage*. Previous related work by Bodin and colleagues extracted the STS stem depth profile by manually defining the anterior and posterior extremities (Bodin et al., 2017). As explained by the authors, defining these extremities automatically was impossible due to the large intersubject variability, particularly at the cross section with the caudal branches of the STS. Using the sulcal pits as landmarks to allow for matching of the sulcus segments across individuals was essential in automatizing the depth profile extraction. It is worth underlining that Leroy et al. (2015) used the *planum temporale* anterior and medial tip as landmarks to identify the STAP. Using the sulcal pits within the STS is certainly more reliable and does not need a manual step. Existing methods quantifying the depth profile were usually applied on the central sulcus of human or non-human primates (Cykowski et al., 2008; Hopkins et al., 2014). They relied on the automatic extraction of the sulci as 3D-morphological objects (Perrot et al., 2011), which sometimes lead to the fusion of adjacent sulci. This problem occurred particularly in the STS due to its various ramifications and frequent interruption by a PP, preventing the extraction of a topologically simple morphological object. Thus, the STS is often seen as segmented in several unconnected pieces (Ochiai et al., 2004) which do not necessarily correspond across individuals. In this context, our method appeared most suitable both to mark off the STAP with sulcal landmarks and quantify the depth profile across individuals without any manual input. Furthermore, the flexibility of our pipeline enabled us to study the presence of PPs splitting other main sulci. Although the sulci of most brain regions were analyzed, we were not able to detect PPs in a few sulci which were either too short to host a pair of sulcal pits or too variable across subjects. For example, we should emphasize the poor group areal boundaries in the occipito-temporal regions (27, 28, 29 Fig. 2), which did not allow us to extract PPs robustly and certainly led to the crossing of true gyri by the SP_{DPF}. Thus, we were not able to investigate further sulcal interruptions in this brain region, which have been reported as being related to reading performance in normal readers and dyslexic subjects (Borst et al., 2016; Im et al., 2016).

Conclusion

The contribution of this paper is twofold. *First*, we defined an automated pipeline composed of sulcal pit extraction on the cortical surface at the individual level, computation of sulcal a pit atlas, geodesic path delineation between any given pair of pits, computation of the depth profile along the bottom of the sulcus, and *pli de passage* detection. We demonstrated the feasibility of such a pipeline in a large dataset to detect PPs and found significant asymmetries in the STAP, dorsal postcentral, rostral intraparietal, and dorsal precentral sulci. *Second*, we demonstrated the genetic influence on PPs located in the left STAP region. Because the STAP is a recent asymmetry appearing in the primate lineage (Leroy et al., 2015), our result confirms that this recent evolutionary change might be related to the emergence of the linguistic network in the left perisylvian region.

Acknowledgments

Data were provided by the Human Connectome Project, WU-Minn Consortium (Principal Investigators: David Van Essen and Kamil Ugurbil; 1U54MH091657) funded by the 16 NIH Institutes and Centers that support the NIH Blueprint for Neuroscience Research; and by the McDonnell Center for Systems Neuroscience at Washington University.

Appendix A. Supplementary data

Supplementary data related to this article can be found at https://doi.org/10.1016/j.neuroimage.2018.03.046.

References

Almasy, L., Blangero, J., 1998. Multipoint quantitative-trait linkage analysis in general pedigrees. Am. J. Hum. Genet. 62, 1198–1211. https://doi.org/10.1086/301844.

Auzias, G., Brun, L., Deruelle, C., Coulon, O., 2015. Deep sulcal landmarks: algorithmic and conceptual improvements in the Definition and extraction of sulcal pits. Neuroimage 111, 12–25. https://doi.org/10.1016/j.neuroimage.2015.02.008.

Bartley, A.J., Jones, D.W., Weinberger, D.R., 1997. Genetic variability of human brain size and cortical gyral patterns. Brain 120, 257–269. https://doi.org/10.1093/brain/120.2.257.

Belin, P., Zatorre, R.J., Lafaille, P., Ahad, P., Pike, B., 2000. Voice-selective areas in human auditory cortex. Nature 403, 309–312. https://doi.org/10.1038/35002078.

Bodin, C., Takerkart, S., Belin, P., Coulon, O., 2017. Anatomo-functional correspondence in the superior temporal sulcus. Brain Struct. Funct. 1–12. https://doi.org/10.1007/s00429-017-1483-2.

Borst, G., Cachia, A., Tissier, C., Ahr, E., Simon, G., Houd, O., 2016. Early cerebral constraints on reading skills in school-age children: an MRI study. Mind, Brain, Educ. 10, 47–54. https://doi.org/10.1111/mbe.12098.

Boucher, M., Whitesides, S., Evans, A., 2009. Depth potential function for folding pattern representation, registration and analysis. Med. Image Anal. 13, 203–214. https://doi.org/10.1016/j.media.2008.09.001.

Calvert, G.A., Bullmore, E.T., Brammer, M.J., Campbell, R., Williams, S.C.R., McGuire, P.K., Woodruff, P.W.R., Iversen, S.D., David, A.S., 1997. Activation of

auditory cortex during silent lipreading. Science 276 (80), 593–596. https://doi.org/10.1126/science.276.5312.593.
Catani, M., Dell'Acqua, F., Vergani, F., Malik, F., Hodge, H., Roy, P., Valabregue, R., Thiebaut de Schotten, M., 2012. Short frontal lobe connections of the human brain. Cortex 48, 273–291. https://doi.org/10.1016/j.cortex.2011.12.001.
Chi, J.G., Dooling, E.C., Gilles, F.H., 1977. Gyral development of the human brain. Ann. Neurol. 1, 86–93. https://doi.org/10.1002/ana.410010109.
Chiarello, C., Vazquez, D., Felton, A., McDowell, A., 2016. Structural asymmetry of the human cerebral cortex: regional and between-subject variability of surface area, cortical thickness, and local gyrification. Neuropsychologia 93, 365–379. https://doi.org/10.1016/j.neuropsychologia.2016.01.012.
Cykowski, M.D., Coulon, O., Kochunov, P.V., Amunts, K., Lancaster, J.L., Laird, A.R., Glahn, D.C., Fox, P.T., 2008. The central sulcus: an observer-independent characterization of sulcal landmarks and depth asymmetry. Cereb. Cortex 18, 1999–2009. https://doi.org/10.1093/cercor/bhm224.
de Juan Romero, C., Bruder, C., Tomasello, U., Sanz-Anquela, J.M., Borrell, V., Romero, C.D.J., Bruder, C., Tomasello, U., Sanz-Anquela, J.M., 2015. Discrete domains of gene expression in germinal layers distinguish the development of gyrencephaly. EMBO J. 34, 1–16. https://doi.org/10.15252/embj.201591176.
de Kovel, C.G.F., Lisgo, S., Karlebach, G., Ju, J., Cheng, G., Fisher, S.E., Francks, C., 2017. Left-right asymmetry of maturation rates in human embryonic neural development. Biol. Psychiatry. https://doi.org/10.1016/j.biopsych.2017.01.016.
Deen, B., Koldewyn, K., Kanwisher, N., Saxe, R., 2015. Functional organization of social perception and cognition in the superior temporal sulcus. Cereb. Cortex 25, 4596–4609. https://doi.org/10.1093/cercor/bhv111.
Dehaene-Lambertz, G., Hertz-Pannier, L., Dubois, J., Meriaux, S., Roche, A., Sigman, M., Dehaene, S., 2006. Functional organization of perisylvian activation during presentation of sentences in preverbal infants. Proc. Natl. Acad. Sci. 103, 14240–14245. https://doi.org/10.1073/pnas.0606302103.
Dehaene, S., Pegado, F., Braga, L.W., Ventura, P., Filho, G.N., Jobert, A., Dehaene-Lambertz, G., Kolinsky, R., Morais, J., Cohen, L., 2010. How learning to read changes the cortical networks for vision and language. Science 330 (80), 1359–1364. https://doi.org/10.1126/science.1194140.
Destrieux, C., Fischl, B., Dale, A., Halgren, E., 2010. Automatic parcellation of human cortical gyri and sulci using standard anatomical nomenclature. Neuroimage 53, 1–15. https://doi.org/10.1016/j.neuroimage.2010.06.010.
DeWitt, I., Rauschecker, J.P., 2012. Phoneme and word recognition in the auditory ventral stream. Proc. Natl. Acad. Sci. 109, E505–E514. https://doi.org/10.1073/pnas.1113427109.
Dubois, J., Benders, M., Cachia, a, Lazeyras, F., Ha-Vinh Leuchter, R., Sizonenko, S.V., Borradori-Tolsa, C., Mangin, J.F., Hüppi, P.S., 2008. Mapping the early cortical folding process in the preterm newborn brain. Cereb. Cortex 18, 1444–1454. https://doi.org/10.1093/cercor/bhm180.
Dubois, J., Poupon, C., Thirion, B., Simonnet, H., Kulikova, S., Leroy, F., Hertz-Pannier, L., Dehaene-Lambertz, G., 2015. Exploring the early organization and maturation of linguistic pathways in the human infant brain. Cereb. Cortex 1–16. https://doi.org/10.1093/cercor/bhv082.
Fischl, B., 2012. FreeSurfer. Neuroimage 62, 774–781. https://doi.org/10.1016/j.neuroimage.2012.01.021.
Frith, C.D., Frith, U., 2007. Social cognition in humans. Curr. Biol. 17, R724–R732. https://doi.org/10.1016/j.cub.2007.05.068.
Galaburda, A.M., Corsiglia, J., Rosen, G.D., Dana, C.A., Sherman, F., Sherman, G.F., 1987. Planum temporale asymmetry, reappraisal since Geschwind and Levitsky. Neuropsychologia 25, 853–868. https://doi.org/10.1016/0028-3932(87)90091-1.
Germanaud, D., Lefèvre, J., Toro, R., Fischer, C., Dubois, J., Hertz-Pannier, L., Mangin, J.F., 2012. Larger is twistier: spectral analysis of gyrification (SPANGY) applied to adult brain size polymorphism. Neuroimage 63, 1257–1272. https://doi.org/10.1016/j.neuroimage.2012.07.053.
Glasel, H., Leroy, F., Dubois, J., Hertz-Pannier, L., Mangin, J.F., Dehaene-Lambertz, G., 2011. A robust cerebral asymmetry in the infant brain: the rightward superior temporal sulcus. Neuroimage 58, 716–723. https://doi.org/10.1016/j.neuroimage.2011.06.016.
Glasser, M.F., Coalson, T.S., Robinson, E.C., Hacker, C.D., Harwell, J., Yacoub, E., Ugurbil, K., Andersson, J., Beckmann, C.F., Jenkinson, M., Smith, S.M., Van Essen, D.C., 2016. A multi-modal parcellation of human cerebral cortex. Nature 536, 171–178. https://doi.org/10.1038/nature18933.
Gómez-Robles, A., Hopkins, W.D., Schapiro, S.J., Sherwood, C.C., 2015. Relaxed genetic control of cortical organization in human brains compared with chimpanzees. Proc. Natl. Acad. Sci. U. S. A. 112, 14799–14804. https://doi.org/10.1073/pnas.1512646112.
Gratiolet, P., 1854. In: Bertrand, Arthus (Ed.), Mémoire sur les plis cérébraux de l'homme et des primates, Paris.
Greve, D.N., Van der Haegen, L., Cai, Q., Stufflebeam, S., Sabuncu, M.R., Fischl, B., Brysbaert, M., 2013. A surface-based analysis of language lateralization and cortical asymmetry. J. Cogn. Neurosci. 25, 1477–1492. https://doi.org/10.1162/jocn_a_00405.
Güntürkün, O., Ocklenburg, S., 2017. Ontogenesis of lateralization. Neuron. https://doi.org/10.1016/j.neuron.2017.02.045.
Habas, P.A., Scott, J.A., Roosta, A., Rajagopalan, V., Kim, K., Rousseau, F., Barkovich, A.J., Glenn, O.A., Studholme, C., 2012. Early folding patterns and asymmetries of the normal human brain detected from in utero MRI. Cereb. Cortex 22, 13–25. https://doi.org/10.1093/cercor/bhr053.
Hein, G., Knight, R.T., 2008. Superior temporal sulcus–It's my area: or is it? J. Cogn. Neurosci. 20, 2125–2136. https://doi.org/10.1162/jocn.2008.20148.
Hilgetag, C.C., Barbas, H., 2006. Role of mechanical factors in the morphology of the primate cerebral cortex. PLoS Comput. Biol. 2, 146–159. https://doi.org/10.1371/journal.pcbi.0020022.
Hopkins, W.D., Meguerditchian, A., Coulon, O., Bogart, S., Mangin, J.-F., Sherwood, C.C., Grabowski, M.W., Bennett, A.J., Pierre, P.J., Fears, S., Woods, R., Hof, P.R., Vauclair, J., 2014. Evolution of the central sulcus morphology in primates. Brain. Behav. Evol. 84, 19–30. https://doi.org/10.1159/000362431.
Huntgeburth, S.C., Petrides, M., 2012. Morphological patterns of the collateral sulcus in the human brain. Eur. J. Neurosci. 35, 1295–1311. https://doi.org/10.1111/j.1460-9568.2012.08031.x.
Hutsler, J.J., 2003. The specialized structure of human language cortex: Pyramidal cell size asymmetries within auditory and language-associated regions of the temporal lobes. Brain Lang. 86, 226–242. https://doi.org/10.1016/S0093-934X(02)00531-X.
Im, K., Jo, H.J., Mangin, J.F., Evans, A.C., Kim, S.I., Lee, J.M., 2010. Spatial distribution of deep sulcal landmarks and hemispherical asymmetry on the cortical surface. Cereb. Cortex 20, 602–611. https://doi.org/10.1093/cercor/bhp127.
Im, K., Raschle, N.M., Smith, S.A., Ellen Grant, P., Gaab, N., 2016. Atypical sulcal pattern in children with developmental dyslexia and at-risk kindergarteners. Cereb. Cortex 26, 1138–1148. https://doi.org/10.1093/cercor/bhu305.
Johnson, M.B., Kawasawa, Y.I., Mason, C.E., Krsnik, Ž., Coppola, G., Bogdanović, D., Geschwind, D.H., Mane, S.M., State, M.W., Šestan, N., 2009. Functional and evolutionary insights into human brain development through global transcriptome analysis. Neuron 62, 494–509. https://doi.org/10.1016/j.neuron.2009.03.027.
Kang, X., Herron, T.J., Ettlinger, M., Woods, D.L., 2015. Hemispheric asymmetries in cortical and subcortical anatomy. Laterality Asymmetries Body, Brain Cogn. 20, 658–684. https://doi.org/10.1080/1357650X.2015.1032975.
Karlebach, G., Francks, C., 2015. Lateralization of gene expression in human language cortex. Cortex 67, 30–36. https://doi.org/10.1016/j.cortex.2015.03.003.
Kochunov, P., Glahn, D.C., Fox, P.T., Lancaster, J.L., Saleem, K., Shelledy, W., Zilles, K., Thompson, P.M., Coulon, O., Mangin, J.F., Blangero, J., Rogers, J., 2010. Genetics of primary cerebral gyrification: heritability of length, depth and area of primary sulci in an extended pedigree of Papio baboons. Neuroimage 53, 1126–1134. https://doi.org/10.1016/j.neuroimage.2009.12.045.
Koelkebeck, K., Miyata, J., Kubota, M., Kohl, W., Son, S., Fukuyama, H., Sawamoto, N., Takahashi, H., Murai, T., 2014. The contribution of cortical thickness and surface area to gray matter asymmetries in the healthy human brain. Hum. Brain Mapp. 35, 6011–6022. https://doi.org/10.1002/hbm.22601.
Le Guen, Y., Auzias, G., Dehaene-Lambertz, G., Leroy, F., Mangin, J.-F., Duchesnay, E., Coulon, O., Frouin, V., 2017a. Regional study of the genetic influence on the sulcal pits. In: 2017 IEEE 14th International Symposium on Biomedical Imaging (ISBI 2017). IEEE, pp. 77–80. https://doi.org/10.1109/ISBI.2017.7950472.
Le Guen, Y., Auzias, G., Leroy, F., Noulhiane, M., Dehaene-Lambertz, G., Duchesnay, E., Mangin, J.-F., Coulon, O., Frouin, V., 2017b. Genetic influence on the sulcal pits: on the origin of the first cortical folds. Cereb. Cortex 1–12. https://doi.org/10.1093/cercor/bhx098.
Le Troter, A., Auzias, G., Coulon, O., 2012. Automatic sulcal line extraction on cortical surfaces using geodesic path density maps. Neuroimage 61, 941–949. https://doi.org/10.1016/j.neuroimage.2012.04.021.
Leroy, F., Cai, Q., Bogart, S.L., Dubois, J., Coulon, O., Monzalvo, K., Fischer, C., Glasel, H., Van der Haegen, L., Bénézit, A., Lin, C.-P., Kennedy, D.N., Ihara, A.S., Hertz-Pannier, L., Moutard, M.-L., Poupon, C., Brysbaert, M., Roberts, N., Hopkins, W.D., Mangin, J.-F., Dehaene-Lambertz, G., 2015. New human-specific brain landmark: the depth asymmetry of superior temporal sulcus. Proc. Natl. Acad. Sci. 112, 1208–1213. https://doi.org/10.1073/pnas.1412389112.
Leroy, F., Glasel, H., Dubois, J., Hertz-Pannier, L., Thirion, B., Mangin, J.-F., Dehaene-Lambertz, G., 2011. Early maturation of the linguistic dorsal pathway in human infants. J. Neurosci. 31, 1500–1506. https://doi.org/10.1523/JNEUROSCI.4141-10.2011.
Li, G., Lin, W., Gilmore, J.H., Shen, D., 2015. Spatial patterns, longitudinal development, and hemispheric asymmetries of cortical thickness in infants from birth to 2 Years of age. J. Neurosci. 35, 9150–9162. https://doi.org/10.1523/JNEUROSCI.4107-14.2015.
Liebenthal, E., Desai, R., Ellingson, M.M., Ramachandran, B., Desai, A., Binder, J.R., 2010. Specialization along the left superior temporal sulcus for auditory categorization. Cereb. Cortex 20, 2958–2970. https://doi.org/10.1093/cercor/bhq045.
Lohmann, G., Von Cramon, D.Y., Colchester, A.C.F., 2008. Deep sulcal landmarks provide an organizing framework for human cortical folding. Cereb. Cortex 18, 1415–1420. https://doi.org/10.1093/cercor/bhm174.
Maingault, S., Tzourio-Mazoyer, N., Mazoyer, B., Crivello, F., 2016. Regional correlations between cortical thickness and surface area asymmetries: a surface-based morphometry study of 250 adults. Neuropsychologia 93, 350–364. https://doi.org/10.1016/j.neuropsychologia.2016.03.025.
Mangin, J.-F., Perrot, M., Operto, G., Cachia, a, Fischer, C., Lefèvre, J., Rivière, D., 2015. Sulcus Identification and Labeling, Brain Mapping: an Encyclopedic Reference. Elsevier Inc. https://doi.org/10.1016/B978-0-12-397025-1.00307-9.
Meng, Y., Li, G., Lin, W., Gilmore, J.H., Shen, D., 2014. Spatial distribution and longitudinal development of deep cortical sulcal landmarks in infants. Neuroimage 100, 206–218. https://doi.org/10.1016/j.neuroimage.2014.06.004.
Mesgarani, N., Cheung, C., Johnson, K., Chang, E.F., 2014. Phonetic feature encoding in human superior temporal gyrus. Science 343 (80), 1006–1010. https://doi.org/10.1126/science.1245994.
Moerel, M., De Martino, F., Formisano, E., 2012. Processing of natural sounds in human auditory cortex: tonotopy, spectral tuning, and relation to voice sensitivity. J. Neurosci. 32, 14205–14216. https://doi.org/10.1523/JNEUROSCI.1388-12.2012.

Moreno, A., Limousin, F., Dehaene, S., Pallier, C., 2018. Brain correlates of constituent structure in sign language comprehension. Neuroimage 167, 151–161. https://doi.org/10.1016/j.neuroimage.2017.11.040.

Nath, A.R., Beauchamp, M.S., 2012. A neural basis for interindividual differences in the McGurk effect, a multisensory speech illusion. Neuroimage 59, 781–787. https://doi.org/10.1016/j.neuroimage.2011.07.024.

Neville, H.J., Bavelier, D., Corina, D., Rauschecker, J., Karni, A., Lalwani, A., Braun, A., Clark, V., Jezzard, P., Turner, R., 1998. Cerebral organization for language in deaf and hearing subjects: biological constraints and effects of experience. Proc. Natl. Acad. Sci. 95, 922–929. https://doi.org/10.1073/pnas.95.3.922.

Ochiai, T., Grimault, S., Scavarda, D., Roch, G., Hori, T., Rivière, D., Mangin, J.-F., Régis, J., 2004. Sulcal pattern and morphology of the superior temporal sulcus. Neuroimage 22, 706–719. https://doi.org/10.1016/j.neuroimage.2004.01.023.

Ocklenburg, S., Arning, L., Gerding, W.M., Epplen, J.T., Güntürkün, O., Beste, C., 2013. FOXP2 variation modulates functional hemispheric asymmetries for speech perception. Brain Lang. 126, 279–284. https://doi.org/10.1016/j.bandl.2013.07.001.

Ono, M., Kubik, S., Abernathey, C., 1990. Atlas of the Cerebral Sulci. Georg Thieme Verlag, Stuggart.

Pallier, C., Devauchelle, A.-D., Dehaene, S., 2011. Cortical representation of the constituent structure of sentences. Proc. Natl. Acad. Sci. 108, 2522–2527. https://doi.org/10.1073/pnas.1018711108.

Paulesu, E., Perani, D., Blasi, V., Silani, G., Borghese, N. a, De Giovanni, U., Sensolo, S., Fazio, F., 2003. A functional-anatomical model for lipreading. J. Neurophysiol. 90, 2005–2013. https://doi.org/10.1152/jn.00926.2002.

Pelphrey, K.A., Viola, R.J., McCarthy, G., 2004. When strangers pass: processing of mutual and averted social gaze in the superior temporal sulcus. Psychol. Sci. 15, 598–603. https://doi.org/10.1111/j.0956-7976.2004.00726.x.

Peper, J.S., Brouwer, R.M., Boomsma, D.I., Kahn, R.S., Hulshoff Pol, H.E., 2007. Genetic influences on human brain structure: a review of brain imaging studies in twins. Hum. Brain Mapp. 28, 464–473. https://doi.org/10.1002/hbm.20398.

Perrot, M., Rivière, D., Mangin, J.-F., 2011. Cortical sulci recognition and spatial normalization. Med. Image Anal. 15, 529–550. https://doi.org/10.1016/j.media.2011.02.008.

Pinel, P., Fauchereau, F., Moreno, A., Barbot, A., Lathrop, M., Zelenika, D., Le Bihan, D., Poline, J.-B., Bourgeron, T., Dehaene, S., 2012. Genetic variants of FOXP2 and KIAA0319/TTRAP/THEM2 locus are associated with altered brain activation in distinct language-related regions. J. Neurosci. 32, 817–825. https://doi.org/10.1523/JNEUROSCI.5996-10.2012.

Redcay, E., Velnoskey, K.R., Rowe, M.L., 2016. Perceived communicative intent in gesture and language modulates the superior temporal sulcus. Hum. Brain Mapp. 37, 3444–3461. https://doi.org/10.1002/hbm.23251.

Régis, J., Mangin, J.-F., Ochiai, T., Frouin, V., Riviére, D., Cachia, A., Tamura, M., Samson, Y., 2005. "Sulcal root" generic model: a hypothesis to overcome the variability of the human cortex folding patterns. Neurol. Med. Chir. 45, 1–17. https://doi.org/10.2176/nmc.45.1 (Tokyo).

Rettmann, M.E., Han, X., Xu, C., Prince, J.L., 2002. Automated sulcal segmentation using watersheds on the cortical surface. Neuroimage 15, 329–344. https://doi.org/10.1006/nimg.2001.0975.

Ringo, J.L., Doty, R.W., Demeter, S., Simard, P.Y., 1994. Time is of the essence: a conjecture that hemispheric specialization arises from interhemispheric conduction delay. Cereb. Cortex 4, 331–343. https://doi.org/10.1093/cercor/4.4.331.

Rogers, J., Kochunov, P., Zilles, K., Shelledy, W., Lancaster, J., Thompson, P., Duggirala, R., Blangero, J., Fox, P.T., Glahn, D.C., 2010. On the genetic architecture of cortical folding and brain volume in primates. Neuroimage 53, 1103–1108. https://doi.org/10.1016/j.neuroimage.2010.02.020.

Schachter, S.C., Ransil, B.J., Geschwind, N., 1987. Associations of handedness with hair color and learning disabilities. Neuropsychologia 25, 269–276. https://doi.org/10.1016/0028-3932(87)90137-0.

Schweizer, R., Helms, G., Frahm, J., 2014. Revisiting a historic human brain with magnetic resonance imaging - the first description of a divided central sulcus. Front. Neuroanat. 8, 35. https://doi.org/10.3389/fnana.2014.00035.

Shattuck, D.W., Joshi, A. a, Pantazis, D., Kan, E., Dutton, R. a, Sowell, E.R., Thompson, P.M., Toga, A.W., Leahy, R.M., 2009. Semi-automated method for delineation of landmarks on models of the cerebral cortex. J. Neurosci. Methods 178, 385–392. https://doi.org/10.1016/j.jneumeth.2008.12.025.

Shen, X., Liu, T., Tao, D., Fan, Y., Zhang, J., Li, S., Jiang, J., Zhu, W., Wang, Y., Wang, Y., Brodaty, H., Sachdev, P., Wen, W., 2018. Variation in longitudinal trajectories of cortical sulci in normal elderly. Neuroimage 166, 1–9. https://doi.org/10.1016/j.neuroimage.2017.10.010.

Specht, K., Wigglesworth, P., 2018. The functional and structural asymmetries of the superior temporal sulcus. Scand. J. Psychol. 59, 74–82. https://doi.org/10.1111/sjop.12410.

Sun, T., Walsh, C. a, 2006. Molecular approaches to brain asymmetry and handedness. Nat. Rev. Neurosci. 7, 655–662. https://doi.org/10.1038/nrn1930.

Tallinen, T., Chung, J.Y., Rousseau, F., Girard, N., Lefèvre, J., Mahadevan, L., 2016. On the growth and form of cortical convolutions. Nat. Phys. 12, 588–593. https://doi.org/10.1038/nphys3632.

Toga, A.W., Thompson, P.M., 2003. Mapping brain asymmetry. Nat. Rev. Neurosci. 4, 37–48. https://doi.org/10.1038/nrn1009.

Toro, R., Perron, M., Pike, B., Richer, L., Veillette, S., Pausova, Z., Paus, T., 2008. Brain size and folding of the human cerebral cortex. Cereb. Cortex 18, 2352–2357. https://doi.org/10.1093/cercor/bhm261.

Turken, A.U., Dronkers, N.F., 2011. The neural architecture of the language comprehension network: converging evidence from lesion and connectivity analyses. Front. Syst. Neurosci. 5, 1–20. https://doi.org/10.3389/fnsys.2011.00001.

Van Essen, D.C., 2005. A Population-Average, Landmark- and Surface-based (PALS) atlas of human cerebral cortex. Neuroimage 28, 635–662. https://doi.org/10.1016/j.neuroimage.2005.06.058.

Van Essen, D.C., Ugurbil, K., Auerbach, E., Barch, D., Behrens, T.E.J., Bucholz, R., Chang, A., Chen, L., Corbetta, M., Curtiss, S.W., Della Penna, S., Feinberg, D., Glasser, M.F., Harel, N., Heath, A.C., Larson-Prior, L., Marcus, D., Michalareas, G., Moeller, S., Oostenveld, R., Petersen, S.E., Prior, F., Schlaggar, B.L., Smith, S.M., Snyder, A.Z., Xu, J., Yacoub, E., 2012. The Human Connectome Project: a data acquisition perspective. Neuroimage 62, 2222–2231. https://doi.org/10.1016/j.neuroimage.2012.02.018.

Zhang, T., Chen, H., Guo, L., Li, K., Li, L., Zhang, S., Shen, D., Hu, X., Liu, T., 2014. Characterization of U-shape streamline fibers: methods and applications. Med. Image Anal. 18, 795–807. https://doi.org/10.1016/j.media.2014.04.005.

Zlatkina, V., Petrides, M., 2014. Morphological patterns of the intraparietal sulcus and the anterior intermediate parietal sulcus of Jensen in the human brain. Proc. R. Soc. B Biol. Sci. 281 https://doi.org/10.1098/rspb.2014.1493, 20141493–20141493.

Zlatkina, V., Petrides, M., 2010. Morphological patterns of the postcentral sulcus in the human brain. J. Comp. Neurol. 518, 3701–3724. https://doi.org/10.1002/cne.22418.